In-situ time-resolved study of structural evolutions in a zirconium alloy during high temperature oxidation and cooling

R. Guillou, Matthieu Le Saux, E. Rouesne, D. Hamon, C. Toffolon-Masclet, D. Menut, Jc Brachet, Jl Bechade, D. Thiaudiere

In-situ time-resolved study of structural evolutions in a zirconium alloy during high temperature oxidation and cooling

R. Guillou[1], M. Le Saux[1,4], E. Rouesne[1], D. Hamon[1], C. Toffolon-Masclet[1], D. Menut[3], J.C. Brachet[1], J.L. Béchade[2], D. Thiaudière[3]

[1] DEN-Service de Recherches Métallurgiques Appliquées (SRMA), CEA, Université Paris-Saclay, F-91191, Gif-sur-Yvette, France

[2] DEN-Service de Recherches de Métallurgie Physique (SRMP), CEA, Université Paris-Saclay, F-91191, Gif-sur-Yvette, France

[3]Synchrotron SOLEIL, F-9192, Gif-sur-Yvette, France
[4]Now at ENSTA Bretagne, UMR CNRS 6027, IRDL, F-29200 Brest, France
raphaelle.guillou@cea.fr, +33 169 084 702

ABSTRACT

In-situ time-resolved Synchrotron X-ray diffraction analyses were performed on zirconium alloy (Zircaloy-4) sheet samples, during their heating, isothermal oxidation at 700, 800 and 900°C under a flowing mixture of He and O_2 and cooling. The oxide growth and the evolution of the oxide structure as a function of time and temperature were studied with suitable time resolution. Oxide layer thicknesses of approximately 10 micrometers were formed during the experiments. The incident X-rays penetrated the whole oxide thickness. The samples were examined after the experiments by field emission gun scanning electron microscopy, electron backscatter diffraction and electron-probe microanalysis. The results showed that the oxide contains a mixture of monoclinic and tetragonal zirconia evolving during heating, oxidation and cooling. The average volume fraction of tetragonal zirconia decreases during oxidation. This fraction is larger at 900°C than at 700 and 800°C. For oxide layers thinner than approximately 5 µm, this fraction is larger at 800°C than at 700°C, but it is rather equivalent for both temperatures when the oxide thickness ranges between 5 and 8 µm. Some of the tetragonal zirconia crystals transforms into the monoclinic phase during cooling after oxidation. This fraction of transformed tetragonal zirconia is larger after oxidation at 900°C than after oxidation at 700 and 800°C. It is suggested that these evolutions of the oxide crystallographic structure are related to micro-stresses and to temperature dependences of the critical size of zirconia crystals below which tetragonal zirconia is stabilized.

Keywords: Zircaloy-4, oxidation, high temperature, zirconia, structure, XRD

1. INTRODUCTION

In some hypothetical accidental scenarios in pressurized water nuclear reactors, such as loss of coolant accidents, fuel cladding tubes made of zirconium-based alloys can be exposed for a few minutes to steam at High Temperature (HT, up to 1200°C) before being cooled and then quenched in water. In such conditions, the cladding material, which is the first barrier for retention of radioactive fission products, undergoes several structural and microstructural evolutions. During oxidation, an oxide layer of ZrO_2 grows on the metal. Depending on temperature, this oxide layer is constituted by the tetragonal structure or a mixture of tetragonal and monoclinic structure [1][2]. The stable phase of pure zirconia below 1170°C is the Monoclinic (M) phase (P21/c space group) but the Tetragonal (T) phase (P42/nmc space group) can be stabilized at lower temperature by stresses or small crystal size [3][4][5][6][7]. Tetragonal zirconia can also be stabilized by elements with a lower valence than zirconium (Zr4+) or a different size [8]. The stabilization may be related to the generation of oxygen vacancies, making the tetragonal phase more energetically favorable [9][10]. Above typically 800°C, depending on the chemical composition of the material and on the thermal history, zirconium progressively transforms from its α_{Zr} phase with a hexagonal close-packed (hcp) structure to its β_{Zr} phase with a body-centered cubic (bcc) structure [11]. At HT, a significant fraction of the oxygen reacting at the metal/oxide interface diffuses into the metallic substrate. Once the solubility limit of oxygen in the β_{Zr} phase is reached, a metallic layer of oxygen-stabilized α_{Zr} phase, called $\alpha_{Zr}(O)$, grows from the interface between the oxide layer and the β_{Zr} phase substrate [11][12][13]. There is a strong through-thickness gradient in oxygen concentration in the $\alpha_{Zr}(O)$ phase layer, from approximately 29 atomic % (at%) at the oxide/$\alpha_{Zr}(O)$ interface down to 10 at% at the $\alpha_{Zr}(O)/\beta_{Zr}$ interface. The underlying metallic layer of β_{Zr} phase, or two-phase $\alpha_{Zr} + \beta_{Zr}$ depending on temperature, has a lower oxygen concentration and a smaller through-thickness gradient, from typically 5 to 1 at%. During cooling, a large fraction of the zirconia tetragonal phase transforms into to the monoclinic phase [2], and the β_{Zr} phase retransforms into hcp phase, the so-called prior-β_{Zr} phase, with a typical Widmanstätten or parallel-lath structure morphology [14]. These structural and microstructural evolutions cause strain fields which induce internal stresses, at both micro and macro scales [15]. Internal stresses generated during oxidation can have an effect on the oxide structure and on the oxidation kinetics of the material. Stresses generated during cooling after oxidation at HT can result in the failure of the metallic part once it is heavily oxidized and/or hydrided [16][17]. To correctly understand the behaviour of the cladding material (oxide and metal) under these conditions, it is therefore necessary to have a good knowledge of the structural evolutions occurring within it. However, to date, these evolutions are poorly quantified for oxidation at HT, above 700°C typically, mainly because they are difficult to characterize in these conditions.

The synchrotron X-Ray Diffraction (XRD) method appears to be suitable to study such structural evolutions. XRD studies performed so far on the oxidation process of zirconium alloys were mainly limited to oxidation temperatures below 500°C, and they were most of the time carried out *post-facto* after cooling down to room temperature [18][19][20][21][22][23][24]. A few XRD experiments were performed at higher temperatures, *e.g.* 650-710°C [25] and 850°C [26]. However, they were most of the time carried out in air. In this case the oxidation of Zr-based alloys at HT is not representative of steam oxidation [27][28][29][30][31][32] due to the strong effect of nitrogen [35][36]. Gosset *et al.* [1][2] have performed a few years ago laboratory *in-situ* XRD analyses during oxidation under O_2-He (to avoid the effect of the nitrogen present in the air) at temperatures between 800 and 1100°C. They have shown in particular that the structure and the microstructure of the growing

oxide layer strongly depend on temperature and cannot be observed *post-facto*, neither at room temperature nor after reheating to the prior oxidation temperature [1][2]. Nevertheless, only a few micrometers of the oxide layer were probed during these analyses. Furthermore, the extended measurement times did not allow following the structural evolutions during the oxidation process with a sufficient time resolution. Indeed, the oxidation process is fast at HT: for instance, for Zircaloy-4 alloy, it only takes 1 min at 900°C in steam to form an approximately 5 µm-thick oxide layer.

This paper presents *in-situ* time-resolved synchrotron X-ray diffraction experiments performed during oxidation at 700, 800 and 900°C in O_2-He and subsequent cooling on Zircaloy-4 sheet samples. The aim of this work was to follow, with suitable time resolution, the oxidation process and to determine the evolution of the structure and the microstructure of the oxide layer as a function of time and temperature. The material and the experimental procedures used for this study are described in Section 2. The results are presented and discussed in Section 3.

2. MATERIAL AND EXPERIMENTAL PROCEDURES

2.1. Material

The experiments were made on stress-relieved annealed low tin Zircaloy-4 sheet samples, with the following composition: 1.3 weight % (wt%) Sn, 0.22 wt% Fe, 0.11 wt% Cr, 0.12 wt% O, Zr balance. Samples of 12 x 12 x 0.6 mm^3 were cut from the sheet. The sample surfaces were then polished with a 600 grit SiC paper and cleaned with ethanol.

2.2 *In situ* synchrotron X-Ray Diffraction (XRD) experiments

In-situ XRD experiments were performed on the DiffAbs (Diffraction and Absorption) beamline of the SOLEIL synchrotron (France). The analyses were carried out in reflection mode with an energy of the X-ray beam fixed to 17.6 keV. This working energy was 400 eV lower than the zirconium K-edge absorption threshold, so that fluorescence was avoided. Using this energy, the penetration depth ranged between approximately 15 and 150 µm depending on the X-ray incidence angle that was greater than the oxide thickness formed during the experiments (approximately 10 µm). The results are thus average measurements over the whole oxide layer thickness. A 300 x 300 μm^2 ray beam size at the center of the 6-circle diffractometer was used in order to obtain good statistics of grains during the analyses. The diffraction patterns were recorded using a XPAD S140 two-dimensional detector (hybrid pixel technology, 560 x 240 $pixels^2$ image size) [39][40]. The detector was placed on the 2θ goniometer arm with a detector/sample distance of 640 mm (Fig. 1). Due to the detector position, only a portion of the Debye Scherrer rings was recorded. Rings radii corresponding to 2θ values (where θ is the Bragg's angle) between 12° and 15° were measured. This encompassed the most significant diffraction reflections of the phases of interest, *i.e.* the $(\bar{1}11)$ (noted (-111) hereinafter) plane family of monoclinic zirconia (2θ = 12.791°) and the (101) plane family of tetragonal zirconia (2θ = 13.511°).

Three temperatures were targeted: 700, 800 and 900°C. The oxidation times were determined in order to obtain an oxide layer thickness of approximately 10 µm at the end of the holding time, according to available oxidation kinetics in steam [32][33] and targeted temperatures. Thus, the following holding times were applied: 180 min at 700°C, 85 min at 800°C and 12 min at 900°C. An Anton Paar DHS 900 heating device was used, with a dome made of PEEK (PolyEtherEtherKetone). The samples were step-heated up to these temperatures, held at these temperatures and finally step-cooled down to room temperature. Two minutes-long isothermal steps were applied every 50°C (from 500°C) during heating and every 20°C during cooling. The diffraction data were measured at each step with 5s counting time per diffraction pattern.
The heating rate and the cooling rate between each step were approximately 20°C/min and 50°C/min, respectively. The average heating rate and cooling rate between room temperature and the oxidation temperature were about 16°C/min and 12°C/min, respectively.

Heating was carried out under primary vacuum (10^{-1} mbar). A mixture of 90% in volume (vol%) He and 10 vol% O_2 was injected during the oxidation and cooling stages. This oxidizing mixture, already used in [1][2][15][37][38], was chosen as a surrogate for steam, excluded for use in the facility. It was checked that the oxidation kinetics of Zircaloy-4 at HT under steam and under O_2 mixed with He are comparable. Despite an absence of hydrogen and a different enthalpy of formation, the oxide formed under 90 vol.% He-10 vol.% O_2 is expected to have properties reasonably similar compared to those of the oxide growing in steam. The flow rate of gas injected in the heating device could not be controlled during these experiments, but measurements of oxide thickness performed after testing (described later in this paper) showed that oxygen supply was sufficient to avoid starvation.

Temperature was monitored using a K-type thermocouple fixed to the sample holder. The actual temperature of the sample could not be measured during the experiments. Nevertheless, it was checked *a posteriori*, through oxide thickness and chemical element distribution measurements that the sample temperature was close to the target temperature, as it will be shown in Section 3.

The two-dimensional Debye-Scherrer ring patterns imaged by the detector were corrected and azimuthally integrated, subsequently to proper calibration using a series of diffraction patterns collected at room temperature on a NIST standard ZnO powder (674b). Each peak of the diffraction line profile was then individually fitted by a simplified Pearson VII function (Eq 1) associated with a linear continuous background [41]:

$$y = a\left(1+\left(\frac{x-d}{b}\right)^2\right)^{-m} \quad (1)$$

with y the intensity, x the angular position, a the maximum intensity of the diffraction peak, d the angular position of the maximum intensity of the peak and b and m two parameters for the Full Width at Half Maximum (FWHM) calculation.

2.6. Characterizations after XRD experiments

The microstructure and the thickness of the oxide layers were observed by Field Emission Gun Scanning Electron Microscopy (FEG-SEM), in backscattered electron mode, using a ZEISS Sigma HD microscope, on polished cross-sections of the samples oxidized during the *in-situ* XRD experiments. Furthermore, oxide grain morphology and crystal orientation were analyzed by Electron BackScatter Diffraction (EBSD). The samples were prepared with special care using an optimized procedure for EBSD analysis.

The distribution of chemical elements within the metallic substrate was examined (spatial resolution of approximately 1 µm) on polished sample cross-sections by Electron-Probe Micro Analysis (EPMA), using a CAMECA SX100 electron microprobe.

3. RESULTS AND DISCUSSION

3.1. Oxide thickness, distribution of chemical elements, temperatures actually achieved

The temperature of the sample was not directly measured during the *in-situ* XRD experiments. Given the heating mode and the thickness of the sample, the temperature at the sample surface was expected to be a little bit lower than the one measured with the thermocouple fixed into the sample holder. In order to estimate the temperature actually reached by the sample, the oxide thickness and the distribution of chemical elements in the metallic substrate were examined and compared to those expected from models established from results of isothermal oxidation tests performed in steam [32][33][34], considering that the oxidation kinetics of the material under steam and under O_2-He are comparable. Average oxide thicknesses of 7.6±1.8 µm, 13.6±3.1 µm and 11.5±1.9 µm were respectively measured after 180 min at approximately 700°C, 85 min at approximately 800°C and 12 min at approximately 900°C (figure 2). The expected oxide layer thicknesses were calculated using a correlation established from results of isothermal oxidation tests performed in steam [32][33]. Oxide growth during heating, isothermal oxidation and cooling was taken into account. The results showed that the average oxide layer thicknesses measured after the experiments could be calculated using this correlation when considering isothermal holding temperatures of approximately 676, 788 and 870°C. This confirms *a posteriori* that the actual temperature of the sample surface (which was not measured during the tests) was not too far from the temperature of the sample holder.

In the case of the sample tested at a target temperature of 700°C, oxygen has diffused through the metallic substrate over approximately 20 µm from the metal-oxide interface (Figure 3a). The examinations revealed that the metal was recrystallized. No sign of phase transformation was evidenced. $Zr(Fe,Cr)_2$ Laves phase precipitates were observed. This is consistent with a temperature around 700°C.

Within the sample for which the sample holder was at 800°C, oxygen has diffused through the metal beneath the oxide over about 30 µm (Figure 3b). Small zones enriched in Fe and Cr were observed. Fe and Cr being β_{Zr}-stabilizers, these zones probably corresponded to regions transformed into β_{Zr} phase during the experiment. At equilibrium, α_{Zr} starts to transform into β_{Zr} at approximately 800°C [11]. These observations showed that the sample has experienced a temperature close to 800°C. According to these observations, a difference smaller than 30°C was estimated.

In the case of 900°C sample holder temperature, oxygen diffusion depth through the metallic substrate was approximately 40-50 µm (Figure 3c). Zones containing Fe concentration higher than 20 wt.% (maximal value measured with a spatial resolution of 1 µm) and Cr concentration higher than 12 wt.% were observed. This showed that the metal partially transformed into β_{Zr}. The volume fraction of β_{Zr} in Zircaloy-4 (with no additional oxygen) expected at equilibrium at 900°C is approximately 60% [11]. The surface fraction of zones enriched in Fe and Cr seemed to be a little lower but not very different. Thus, it could be concluded from these observations that the temperatures of the samples during the experiments were close to the target temperatures.

The oxygen concentration profiles measured after the experiments are compared in Fig. 3 to the profiles calculated with the model presented in [34], considering a semi-infinite system and the diffusion coefficient of oxygen, in the hcp Zircaloy-4. Oxygen diffusion during heating and cooling was not taken into account, as a first approximation since the time spent at high temperature during heating and cooling was small compared to the plateau duration. The calculations were performed for isothermal oxidation at 700, 800 and 900°C. The comparison between calculated and measured profiles reinforces the conclusion that the actual temperature of the sample was close to the target temperature.

3.2. Oxide microstructure after cooling

Microstructure of the oxide layers formed during the experiments was examined by FEG-SEM and EBSD (Figure 2). One should keep in mind that these observations were performed after cooling down to room temperature. Thus, they are not necessarily representative of the oxide microstructure at HT before cooling: phase transformation can occur and oxide can be damaged during cooling, under the effect of internal stresses generated from phase transformations of the metal and the oxide, and from differences between the thermal coefficients of the different phases/layers constituting the oxidized cladding material [15].

Both equiaxed and columnar grains are observed after oxidation at approximately 700°C, with a size between typically 100 and 200 nm (Figure 2a)). The metal-oxide interface appeared undulated. Micro-cracks parallel to the metal-oxide interface were observed within the oxide layer, preferentially where the layer was the thinner (crests of the waves of the undulated metal-oxide interface with the oxide upward). It can be assumed that these pores and cracks were not interconnected and acted as barriers against transport of oxidizing species from the outer atmosphere to the metal and/or have formed during cooling rather than during oxidation. The undulation of the metal-oxide interface is probably associated with stress levels lower in average than those expected for a metal-oxide interface without undulation, but also with more heterogeneous stress fields [44][45]: compressive stresses in the oxide in the directions parallel to the oxide outer surface are expected to be the highest at the wave crest, where radial stresses are positive while they are negative at the wave trough. The locations where cracks parallel to the metal-oxide interface were observed are consistent with such stress fields, assuming that cracks form perpendicular to the maximum principal stress, as expected for brittle materials. The transport of oxygen to the metal may be slowed down due to the higher compressive stresses expected at the wave crests (due to a decrease in oxygen vacancy mobility [43]) or to particular characteristics of the oxide in these zones.

As shown in figure 2b), the grains of the oxide layer formed at about 800°C were rather equiaxed and small (approximately 100 to 200 nm) at the outer periphery of the layer (over about 3 µm from the outer surface). The oxide closer to the metal-oxide interface showed a more columnar structure, with grains, a few hundreds of nanometers wide and a few micrometers long, mainly oriented perpendicularly to the metal/oxide interface. The

closer to the metal-oxide interface, the larger the grains. Examinations suggested the existence of several crystal variants of monoclinic zirconia in some of the columnar grains, revealing that a phase transformation has occurred (during oxidation and/or cooling). Crystal variants and crystal orientation relations between tetragonal and monoclinic phases will not be further discussed in this paper and will be addressed in another paper. Grains without variant were observed, preferentially near the metal-oxide interface where the oxide was the thicker (wave troughs of the undulated metal-oxide interface). As in the case of the oxide formed at approximately 700°C, the observations revealed cracks parallel to the metal-oxide interface in front of the wave crests of the undulated metal-oxide interface.

Similar observations were made for the oxide formed at about 900°C (Figure 2c)). Nevertheless, grains appeared to be a little coarser and cracks appeared to be less numerous and smaller than in the case of oxide layers formed at 700 and 800°C.

These observations showed that:

- the oxide crystal size increased in the course of oxidation,
- zirconia structure and microstructure were heterogeneous within the oxide layer.

Furthermore, the presence of several crystal variants of zirconia suggests that zirconia was partly tetragonal during oxidation and that a fraction of this tetragonal zirconia transformed into monoclinic zirconia during oxidation and/or during cooling (martensitic transformation). This is discussed hereinafter in light of the *in-situ* XRD experiments presented.

3.3 *In-situ* analysis of structural evolutions during heating, oxidation and cooling

The oxidation process of the material and the evolution of the structure of zirconia were followed *in-situ* by synchrotron XRD during heating, isothermal holding and cooling. One should keep in mind that the penetration depth was between 15 and 150 µm, so that the whole oxide layer and a part of the underlying metal were analyzed. As a consequence, the diffraction data presented hereinafter are an average of the information over the whole oxide layer thickness (lower than 15 µm).

Figure 4 shows typical diffraction images recorded before heating, after oxidation at the end of isothermal holding and after cooling. The corresponding diffraction patterns obtained by azimuthal integration of the 2D frame are also shown. The reflections corresponding to zirconium and to monoclinic and tetragonal zirconia can be clearly observed. Tetragonal zirconia diffraction peaks corresponding to the native zirconia layer (thickness of a few nanometer) are observed at room temperature before heating. Examples of diffraction patterns obtained during step-heating (20°C/min heating rate, 2 min-long isothermal plateaus every 50°C) are given in figure 5.

The results show that zirconia grows during heating (the intensity of the diffraction peaks of zirconia increases). Indeed, heating was carried out under primary vacuum and zirconium reacted with the (small) amount of residual oxygen. The intensities of monoclinic and tetragonal zirconia diffraction peaks continuously increased during heating, as an illustration of growth of the oxide layer. The results confirmed that tetragonal zirconia can be

stabilized during oxidation, even at relatively low temperature. Zirconia diffraction peaks tend to become narrower during heating (figure 5) probably because zirconia crystals tend to become coarser in average.

Examples of diffraction patterns recorded during isothermal oxidation under mixture of 90% in volume (vol%) He and 10 vol% O_2 at approximately 700, 800 and 900°C are given in figure 6. The intensities of zirconia peaks grow during isothermal holding as a result of the oxidation process. The width of the zirconia diffraction peaks diminishes during oxidation. This shows that crystals became larger in average. Furthermore, diffraction peaks of tetragonal zirconia tend to be wider in average than those of monoclinic zirconia, suggesting that tetragonal crystals are smaller. Given the conditions of the experiments which have not been optimized regarding this aspect, it is tricky to provide truly quantitative results on crystal size. It would be interesting to perform dedicated experiments to derive more quantitative results on crystal size.

To determine the tetragonal zirconia phase mean volume fraction, the widely used Garvie-Nicholson formula [42] was applied:

$$f_T = \frac{I_{T(101)}}{I_{T(101)} + I_{M(111)} + I_{M(-111)}} \quad (2)$$

where $I_{T(101)}$, $I_{M(111)}$ and $I_{M(-111)}$ are respectively the maximum intensities of the (101) tetragonal zirconia reflection and the (111) and (-111) monoclinic zirconia reflections. This commonly used formula relies on strong assumptions. In particular, it is considered that the crystallographic texture of the material has no significant effect on the result. The evaluation of the volume fraction of tetragonal zirconia using this formula is probably approximate.

As shown in Fig. 7, the volume fraction of tetragonal zirconia decreases during heating. Figure 8 represents the evolution of the tetragonal phase volume fraction calculated for the three target oxidation temperatures (700, 800 and 900°C) as a function of the oxidation time or the expected oxide thickness. The expected oxide layer thickness was calculated as a function of time using the aforementioned correlation from [32] and considering isothermal holding temperatures of 676, 788 and 870°C (as the actual temperature of the sample surface was not measured during the tests and it was probably not exactly equal to the temperature of the sample holder). It can be observed that the average amount of zirconia tetragonal phase is higher at approximately 900°C than at 700 and 800°C for a similar oxidation time or oxide thickness. The tetragonal phase volume fraction is lower at 800°C than at 700°C for a given oxidation time but it is higher for a given oxide thickness, below approximately 5 µm. For oxide thicknesses between 5 and 8 µm, the tetragonal phase volume fractions are close at 700 and 800°C.

The higher the temperature, the closer it is to the temperature range in which tetragonal zirconia is thermodynamically stable (*i.e.* in the absence of stabilizing factors). Tetragonal zirconia can be stabilized when the crystal size is below a critical value [43][44][45]. This stabilization by small crystal size is assumed to be due to the generation of excess oxygen vacancies within small crystals and to the lower surface free energy of tetragonal zirconia [9][10]. The crystal size critical value is expected to increase with the increase of temperature [44][45]. The average value and the width of the crystal size distribution for the two phases increase with increasing the oxidation temperature (Fig. 9), and micro-stresses are assumed to decrease. The slight decrease of the tetragonal zirconia volume fraction during heating may be related to the growth of zirconia crystals, which

become larger with increasing temperature. The increase of the fraction of tetragonal zirconia with increasing the plateau oxidation temperature may be explained by assuming that the increase of temperature is associated with an increase of the average crystal size smaller than the increase of the critical crystal size below which tetragonal zirconia stabilizes (Fig. 10).

At the beginning of the isothermal holdings at about 900, 800 and 700°C, the tetragonal phase volume fractions were approximately 60%, 30% and 40%, respectively. For the three oxidation temperatures, a decrease of several percent of the average volume fraction of the tetragonal phase was observed during oxidation. This tendency is probably related to an increase of the crystal size (Fig. 11) and to a decrease of the average stress level during oxidation. The observed decrease, during oxide growth, of the difference between tetragonal zirconia volume fractions obtained at approximately 700°C and 800°C can be related to an increase of the average crystal size (relatively to the critical crystal size below which tetragonal zirconia is stabilized) during oxidation more pronounced at 700°C compared to 800°C, in addition to a less significant decrease of micro-stress levels at 700°C compared to 800°C.

The volume fraction of tetragonal zirconia estimated for the oxidation carried out (in a He-O_2 mixture) at approximately 700°C is a few percent larger than the one reported by Platt *et al.* [25] for Zircaloy-4 oxidized during 42 to 82 min in air at 710°C. The values of tetragonal phase volume fraction obtained in the case of oxidation performed at approximately 800 and 900°C are relatively consistent (for the oxide layer thicknesses within the range investigated here) with the volume fraction of about 20% estimated by Valot *et al.* [26] from laboratory *in-situ* XRD on polycrystalline zirconium oxidized under pure oxygen at 850°C.

In order to investigate how the absolute amount of tetragonal zirconia evolves during oxidation and try to identify the mechanism responsible for the decrease of tetragonal phase volume fraction, an “equivalent” tetragonal zirconia thickness was calculated. It corresponds to the product of the expected “instantaneous” total oxide thicknesses calculated using the aforementioned correlation by the “instantaneous” tetragonal phase volume fraction deduced from the XRD data. The results are shown in figure 12. The “equivalent” thickness of tetragonal zirconia is 2-3 times larger at 900°C than at 700 and 800°C, for a given total oxide thickness. The “equivalent” thickness of tetragonal zirconia rapidly increased at the beginning of oxidation and then stabilized. Indeed, at the beginning of oxidation, zirconia crystals forming at the oxide-metal interface were very small and internal micro-stresses may be very high so that zirconia may be mainly tetragonal. Then, in the course of oxidation, zirconia crystals became larger and micro-stresses tended to decrease. These evolutions may lead to

- a decrease of the fraction of zirconia nucleating with a tetragonal structure,
- a destabilization of a part of the tetragonal phase which therefore transforms into the monoclinic phase, in particular when moving away from the oxide-metal interface

Figure 13 shows the evolution of the tetragonal phase volume fraction during step-cooling. The tetragonal phase volume fraction progressively decreased in the course of cooling. This shows that some of the tetragonal zirconia crystals transformed into the monoclinic phase and/or that zirconia forming during cooling was mostly monoclinic. After oxidation at approximately 900°C, almost all tetragonal zirconia transformed into monoclinic zirconia during cooling so that the residual volume fraction of tetragonal zirconia was low at room temperature (approximately 2%). The tetragonal phase fraction also decreased during cooling after oxidation at

approximately 700 and 800°C but the decrease was significantly smaller (a few percent). The residual fraction of tetragonal zirconia at room temperature was approximately 5% after cooling from 800°C, *i.e.* higher than the residual fraction obtained after cooling from 900°C. These tendencies during cooling are consistent with those obtained by Gosset *et al.* [2] using laboratory *in-situ* XRD. In this last case, only the few outer microns of the oxide layer could have been analyzed with measurement times of 500s. In the present case, the whole oxide layer was analyzed with only 1s-long measurements, so that the oxidation process could be analyzed with a relevant time-resolution. Again, these results may be explained by considering the evolution as a function of temperature of the critical crystal size for stabilization of tetragonal zirconia. Zirconia crystals were larger in average (with a wider size distribution) after oxidation at 900°C than after oxidation at lower temperatures (Fig. 9). The critical crystal size below which tetragonal zirconia is stabilized decreases during cooling (Fig. 10). The higher the oxidation temperature, the larger the crystal size and the smaller the fraction of zirconia crystals having a size that remains below the critical size during cooling.

In accordance with the *post-mortem* observations previously presented, the results of XRD analyses show an increase of the oxide grain size and highlight the presence of tetragonal zirconia during oxidation, and the transformation of a fraction of this tetragonal zirconia into monoclinic zirconia during oxidation and/or during cooling.

4. CONCLUSIONS

In-situ time-resolved Synchrotron XRD analyses were performed on Zircaloy-4 sheet samples, during their heating, oxidation at approximately 700, 800 and 900°C under a flowing mixture of He and O_2 and final cooling. It was possible to follow the oxide growth with a suitable time resolution and determine the evolution of the structure of the oxide as a function of time and temperature. Oxide layer thicknesses around ten micrometers were formed at the end of the experiments. The whole oxide thickness was probed by X-rays. Thanks to post-mortem characterizations of the samples by EPMA and SEM, it was checked that the control of the temperature and of the oxidizing atmosphere was satisfactory during the experiments. The results showed that the oxide is composed of both monoclinic and tetragonal zirconia. The average proportion of the tetragonal phase of zirconia decreases during oxidation. The volume fraction of tetragonal zirconia is larger at 900°C than at 700 and 800°C. It is larger at 800°C than at 700°C while the oxide layer is thinner than approximately 5 µm. For oxide layer thicknesses between about 5 and 8 µm, the volume fractions of tetragonal zirconia at 700 and 800°C are close. Furthermore, it was shown that a fraction of the tetragonal zirconia formed during the oxidation transforms into monoclinic zirconia during cooling. The proportion of tetragonal zirconia that transforms into monoclinic zirconia during cooling is much larger after oxidation at 900°C than after oxidation at 700 and 800°C. The evolutions of the structure of the oxide observed during oxidation and cooling may be explained by considering the temperature dependences of the size of zirconia crystals and the critical crystal size below which tetragonal zirconia is stabilized. Furthermore, micro-stresses within the oxide may play a significant role on the oxide structure and microstructure. The feasibility of accurate measurement of these sizes and these stresses as well as their evolution is under investigation.

5. ACKNOWLEDGEMENTS

This work is funded by the French nuclear institute (CEA, EDF and Framatome) in the framework of the GAINES project. We also thank Cristian Mocuta, beamline scientist at DiffAbs beamline, for his help for the python script he provided for the 2D image corrections.

References

[1] D. Gosset, M. Le Saux, D. Simeone, D. Gilbon, New insights in structural characterisation of zirconium alloys oxidation at high temperature, Journal of Nuclear Materials 429 (2012) 19-24.

[2] D. Gosset, M. Le Saux, In-situ X-ray diffraction analysis of zirconia layer formed on zirconium alloys oxidized at high temperature, Journal of Nuclear Materials 458 (2015) 245-252.

[3] R.C. Garvie, Stabilization of the tetragonal structure of zirconia microcrystals, The Journal of Physical Chemistry, 82 (1978) 218-224.

[4] G. Baldinozzi, D. Simeone, D. Gosset, M. Dutheil, Neutron Diffraction Study of the Size-Induced Tetragonal to Monoclinic Phase Transition in Zirconia Nanocrystals, Physical Review Letters 90 (2003) 216103-1-4.

[5] I. Kasatkin, F. Girgsdies, T. Ressler, R.A. Caruso, J.H. Schattka, J. Urban, K. Weiss, HRTEM observation of the monoclinic-to-tetragonal (m-t) phase transition in nanocrystallite ZrO_2, Journal of Nuclear Sciences 39 (2004) 2151-2157.

[6] R.C. Garvie, M.V. Swain, Thermodynamics of the tetragonal to monoclinic phase transformation in constrained zirconia microcrystals – Part 1 In the absence of an applied stress field, Journal of Materials Science 20 (1985) 1193-1200.

[7] R.C. Garvie, Thermodynamics of the tetragonal to monoclinic phase transformation in constrained zirconia microcrystals – Part 2 In the presence of an applied stress field, Journal of Materials Science 20 (1985) 3479-3486.

[8] P. Li, I.W. Chen, J.E. Penner-Hahn, Effect of dopants on zirconia stabilization - An X-ray absorption study: I, trivalent dopants, Journal of the American Ceramic Society 77 (1994) 118-128.

[9] S. Shukla, S. Seal, Mechanisms of room temperature metastable tetragonal phase stabilisation in zirconia. International Materials Reviews 50 (2005) 45-64.

[10] S. Fabris, A.T. Paxton, M.W. Finnis, A stabilization mechanism of zirconia based on oxygen vacancies only. Acta Materialia 50 (2002) 5171-5178

[11] J.C. Brachet, L. Portier, T. Forgeron, J. Hivroz, D. Hamon, T. Guilbert, T. Bredel, P. Yvon, J.P. Mardon, P. Jacques, Influence of hydrogen content on the α/β phase transformation temperatures and on the thermal-mechanical behavior of Zy-4, M4 (ZrSnFeV), and M5™ (ZrNbO) alloys during the first phase of LOCA transient, Zirconium in the Nuclear Industry: 13th International Symposium, June 10-14 2001, Annecy, France, ASTM STP 1423, American Society for Testing and Materials, West Conshohocken, PA, 2002, pp. 673-701.

[12] A. Sawatzky, G.A. Ledoux, S. Jones, Oxidation of Zirconium during a High-Temperature Transient, Zirconium in the Nuclear Industry, ASTM STP633, A. L. Lowe, Jr. and G. W. Parry, Eds., ASTM International, Philadelphia, PA, 1977, pp. 134-149.

[13] H.M. Chung, A.M. Garde, T.F. Kassner, Development of an Oxygen Embrittlement Criterion for Zircaloy Cladding Applicable to Loss-of-Coolant Accident Conditions in Light-Water Reactors, Zirconium in the Nuclear Industry, ASTM STP681, J. H. Schemel and T. P. Papazoglou, Eds., ASTM International, Philadelphia, PA, 1979, pp. 600-627.

[14] O.T. Woo, K. Tangri, Transformation Characteristics of Rapidly Heated and Quenched Zircaloy-4-Oxygen Alloys. Journal of Nuclear Materials 79 (1979) 83-94.

[15] M. Le Saux, T. Guilbert, J.C. Brachet, An approach to study oxidation-induced stresses in Zr alloys oxidized at high temperature, Corrosion Science 140 (2018) 79-91.

[16] M. Billone, Y. Yan, T. Burtseva, R. Daum, Cladding Embrittlement during Postulated Loss-of-Coolant Accidents, NUREG/CR-6967, Argonne National Laboratory, Lemont, IL, 2008.

[17] F. Nagase, T. Fuketa, Behavior of Pre-Hydrided Zircaloy Cladding under Simulated LOCA Conditions, Journal of Nuclear Science and Technology 42 (2005) 209-218.

[18] G. David, R. Geschier, C. Roy, Etude de la croissance de l'oxyde sur le zirconium et le Zircaloy-2, Journal of Nuclear Materials 38 (1971) 329-339.

[19] J. Godlewski, How the Tetragonal Zirconia is Stabilized in the Oxide Scale that is Formed on a Zirconium Alloy Corroded at 400°C in Steam, in: Zirconium in the Nuclear Industry: Tenth International Symposium, ASTM STP 1245, A.M. Garde and E.R. Bradley, Eds., American Society for Testing and Materials, Philadelphia, 1994, pp. 663-684.

[20] J.L. Béchade, M. Gailhanou, P. Goudeau, P. Yvon, X-ray determination of residual stresses and phase quantification in ZrO_2 oxide layers formed on Zircaloy-4, High Temp Material Processes 2 (1998) 359-367.

[21] N. Pétigny, P. Barberis, C. Lemaignan, C. Valot, M. Lallemant, In situ XRD analysis of the oxide layers formed by oxidation at 743 K on Zircaloy-4 and Zr-1NbO, Journal of Nuclear Materials 280 (2000) 318-330.

[22] J.L. Béchade, R. Brenner, P. Goudeau, M. Gailhanou, Determination of residual stresses in a zirconia layer by X-ray diffraction and by a micromechanical approach: thermoelastic anisotropy effect, Revue de Métallurgie 100 (2003) 1151-1156.

[23] E. Polatidis, P. Frankel, J. Wei, M. Klaus, R.J. Comstock, A. Ambard, S. Lyon, R.A. Cottis, M. Preuss, Residual stresses and tetragonal phase fraction characterization of corrosion tested Zircaloy-4 using energy dispersive synchrotron X-ray diffraction, Journal of Nuclear Materials 432 (2013) 102-112.

[24] H. Swan, M.S. Blackmur, J.M. Hyde, A. Laferrere, S.R. Ortner, P.D. Styman, C. Staines, M. Gass, H. Hulme, A. Cole-Baker, P. Frankel, The measurement of stress and phase fraction distributions in pre and post-transition Zircaloy oxides using nano-beam synchrotron X-ray diffraction, Journal of Nuclear Materials 479 (2016) 559-575.

[25] P. Platt, E. Polatidis, P. Frankel, M. Klaus, M. Gass, R. Howells, M. Preuss, A Study into Stress Relaxation in Oxides Formed on Zirconium Alloys, Journal of Nuclear Materials 456 (2015) 415-425.

[26] C. Valot, D. Ciosmak, M. Lallemant, Spatiotemporal dynamics in the oxidation of groups IV-V metals: study of zirconium, Solid State Ionics 101-103 (1997) 769-774.

[27] L. Baker, L.C. Just, Studies of Metal-Water Reactions at High Temperatures. III. Experimental and Theoretical Studies of the Zirconium-Water Reaction, ANL-6548, Argonne National Laboratory, Lemont, IL, 1962.

[28] J.V. Cathcart, R.E. Pawel, R.A. McKee, R.E. Druschel, G.J. Yurek, J.J. Campbell, S.H. Jury, Zirconium Metal-Water Oxidation Kinetics IV. Reaction Rate Studies, ORNL/NUREG-17, US Nuclear Regulatory Commission, Washington, D.C, 1977.

[29] F. Nagase, T. Otomo, H. Uetsuka, Oxidation Kinetics of Low-Sn Zircaloy-4 at the Temperature Range from 773 to 1573K, Journal of Nuclear Science and Technology 40 (2003) 213-219.

[30] J.H. Baek, K.B. Park, Y.H. Jeong, Oxidation kinetics of Zircaloy-4 and Zr-1Nb-1Sn-0.1Fe at temperatures of 700-1200°C, Journal of Nuclear Materials 335 (2004) 443-456.

[31] L. Portier, T. Bredel, J.C. Brachet, V. Maillot, J.P. Mardon, A. Lesbros, Influence of Long Service Exposures on the Thermal-Mechanical Behaviour of Zy-4 and M5™ Alloys in LOCA Conditions, Journal of ASTM International 2 (2005) JAI12468.

[32] M. Le Saux, V. Vandenberghe, P. Crébier, J.C. Brachet, D. Gilbon, J.P. Mardon, B. Sebbari, Influence of Steam Pressure on the High Temperature Oxidation and Post-Cooling Mechanical Properties of Zircaloy-4 and M5™ Cladding (LOCA Conditions), Zirconium in the Nuclear Industry: 17th Volume, STP1543, B. Comstock and P. Barbéris, Eds., ASTM International, West Conshohocken, PA, 2014, pp. 1002-1053.

[33] M. Le Saux, J.C. Brachet, V. Vandenberghe, E. Rouesne, S. Urvoy, A. Ambard, R. Chosson (2019). Effect of a pre-oxide on the high temperature steam oxidation of Zircaloy-4 and M5 alloys. Submitted to Journal of Nuclear Materials.

[34] X. Ma, C. Toffolon-Masclet, T. Guilbert, D. Hamon, J.C. Brachet, Oxidation kinetics and oxygen diffusion in low-tin Zircaloy-4 up to 1523 K, Journal of Nuclear Materials 377 (2008) 359-369.

[35] C. Duriez, T. Dupont, B. Schmet, F. Enoch, Zircaloy-4 and M5® high temperature oxidation and nitriding in air, Journal of Nuclear Materials 380 (2008) 30-45.

[36] M. Steinbrück, M. Böttcher, Air oxidation of Zircaloy-4, M5™ and ZIRLO™ cladding alloys at high temperatures, Journal of Nuclear Materials 414 (2011) 276-285.

[37] H. Uetsuka, P. Hofmann, High-temperature oxidation kinetics of Zircaloy-4 in oxygen/argon mixtures Journal of Nuclear Materials, 168 (1989) 47-57

[38] M. Steinbrück, Oxidation of zirconium alloys in oxygen at high temperatures up to 1600°C, Oxidation of Metals, 70 (2008) 317-329

[39] S. Basolo, J.F. Berar, N. Boudet, P. Breugnon, B. Chantepie, J.C. Clemens, P. Delpierre, B. Dinkespiler, S. Hustache, K. Medjoubi, M. Menouni, C. Morel, P. Pangaud, E. Vigeolas, A 20 kpixels CdTe photon-counting imager using XPAD chip, Nuclear Instruments and Methods A 589 (2008) 268–274

[40] C. Le Bourlot, P. Landois, S. Djaziri, P.O. Renault, E. Le Bourhis, P. Goudeau, M.Pinault, M. Mayne-L'Hermite, B. Bacroix, D. Faurie, O. Castelnau, P. Launois, S., Rouziere, Synchrotron X-ray diffraction experiments with a prototype hybrid pixel detector, Journal of Applied Crystallography 45 (2012) 38-47

[41] V. Pecharsky, P. Zavalij, Fundamentals of Powder Diffraction and Structural Characterization of Materials, Second Edition, Springer US publisher (2009)

[42] R.C. Garvie, P.S. Nicholson, Phase analysis in zirconia systems, Journal of the American Ceramic Society 55 (1972) 303-305.

[43] K. Sato, K. Suzuki, R. Narumi, K. Yashiro, T. Hashida, J. Mizusaki, Ionic Conductivity in Uniaxial Micro Strain/Stress Fields of Yttria-Stabilized Zirconia, Japanese Journal of Applied Physics 50 (2011) 055803.

[44] M. Parise, O. Sicardy, G. Cailletaud, Modelling of the mechanical behavior of the metaloxide system during Zr alloy oxidation, Journal of Nuclear Materials 256 (1998) 35-46.
[45] V. Optasanu, L. Raceanu, T. Montesin, Simulation of Metal/Oxide Interface Mobility: Effects of Mechanical Stresses on Geometrical Singularities, Defect and Diffusion Forum 323-325 (2012) 109-114.

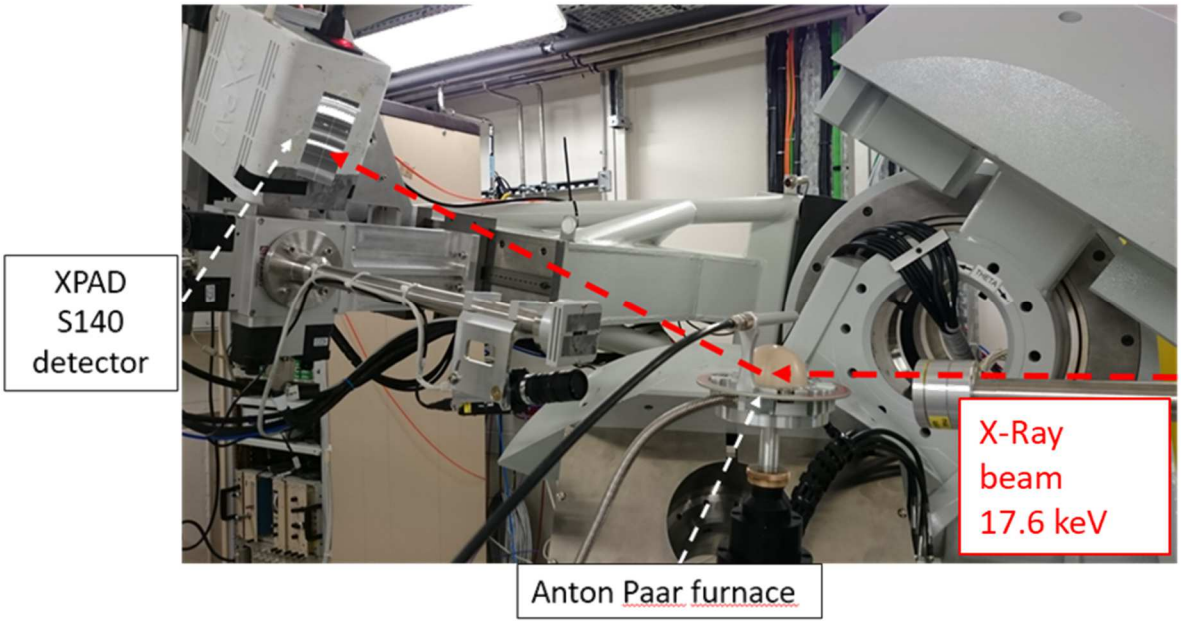

Fig. 1. Experimental setup for XRD experiments.

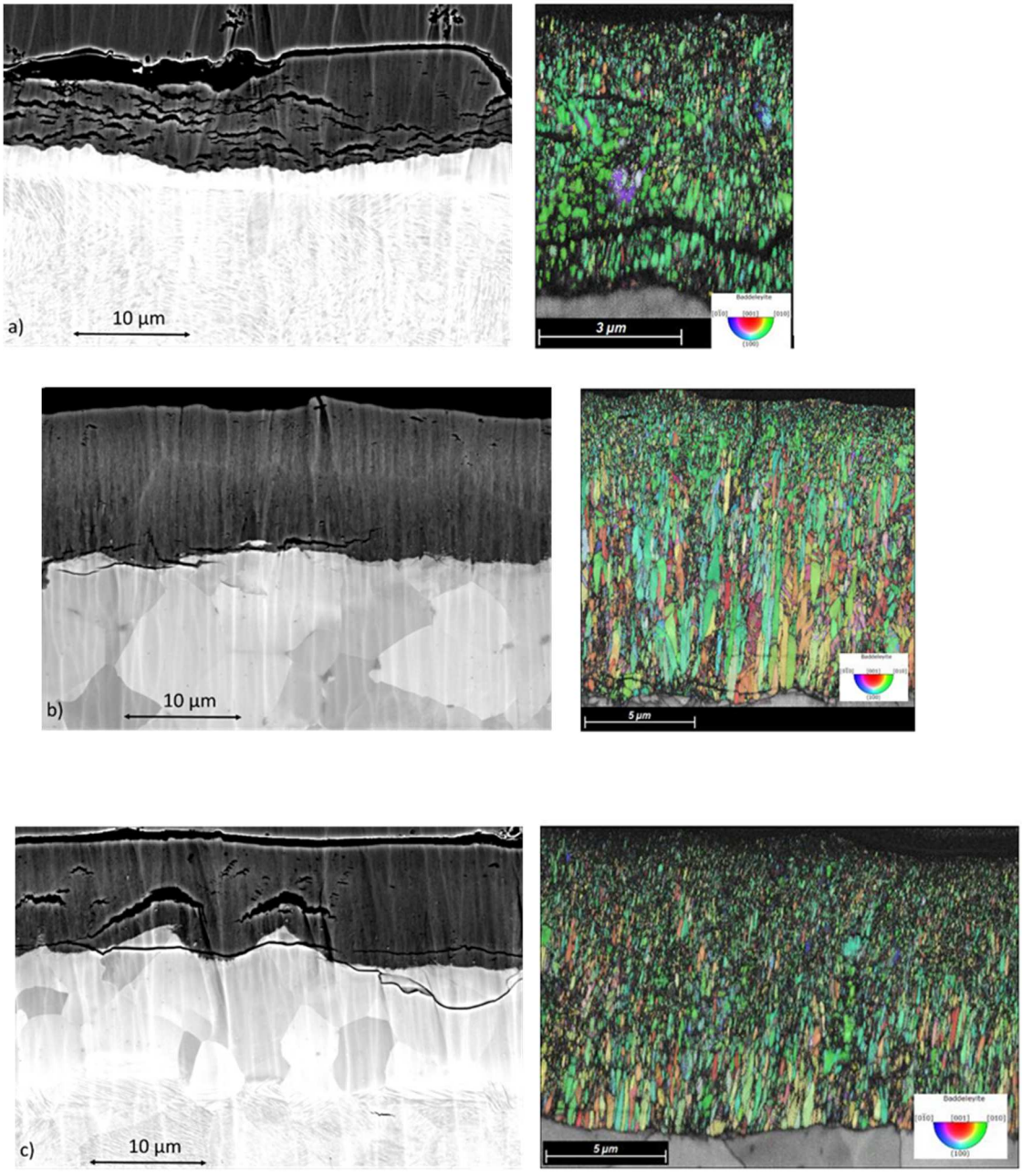

Fig. 2. SEM (back scattered electron mode) micrographs (on the left) and EBSD crystal orientation maps (on the right) (focusing on zirconia layer) of cross-sections of samples oxidized a) 180 min at about 700°C, b) 85 min at about 800°C and c) 12 min at about 900°C (scale of the crystal orientation map not the same in a) than in b) and c)).

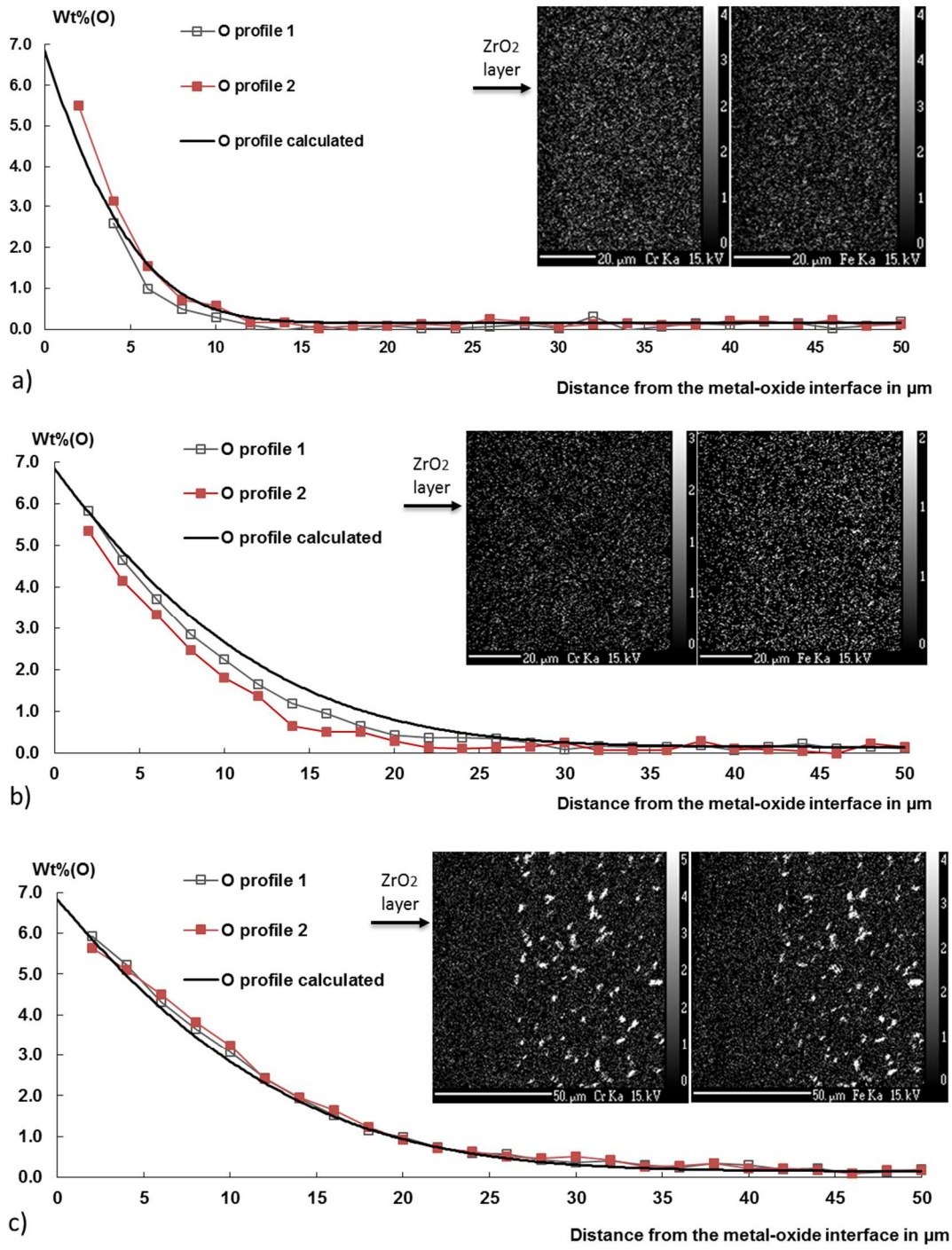

Fig. 3. Oxygen concentration profiles (EPMA) of oxygen (two profiles measured at different positions) in the metallic substrate of samples oxidized a) 180 min at about 700°C, b) 85 min at about 800°C and c) 12 min at about 900°C; comparison to oxygen concentration profiles calculated by considering an isothermal oxidation of 180 min at 700°C, 85 min at 800°C and 12 min at 900°C. X-ray maps of Cr and Fe in the metal beneath the metal-oxide interface of samples.

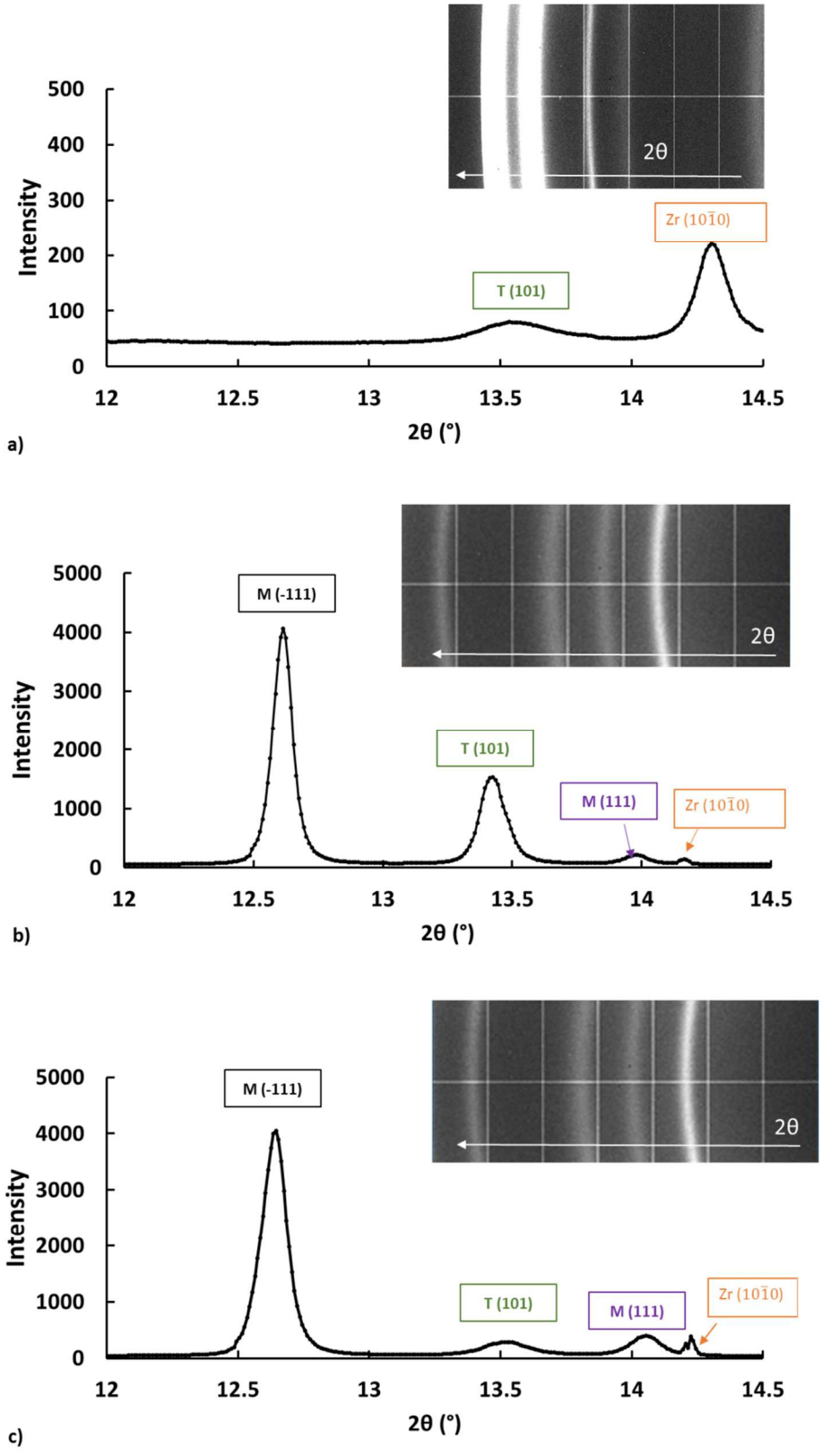

Fig. 4. Examples of 2D diffraction images recorded a) before heating, b) after 12 min-long oxidation at 900°C and c) after cooling ; corresponding diffraction patterns obtained by azimuthal integration.

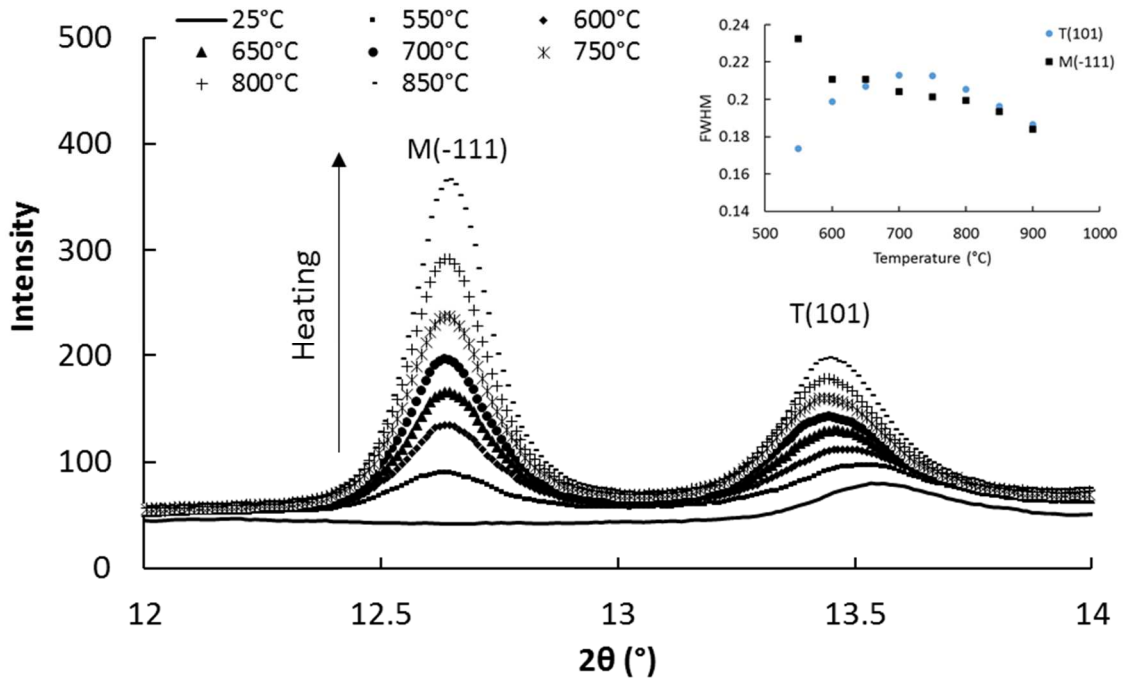

Fig. 5. Diffraction patterns obtained during step-heating up to approximately 900°C (20°C/min heating rate, 2 min-long isothermal steps every 50°C from 550°C) under primary vacuum; evolution of the FWHM of the two main peaks of zirconia as a function of temperature during step-heating.

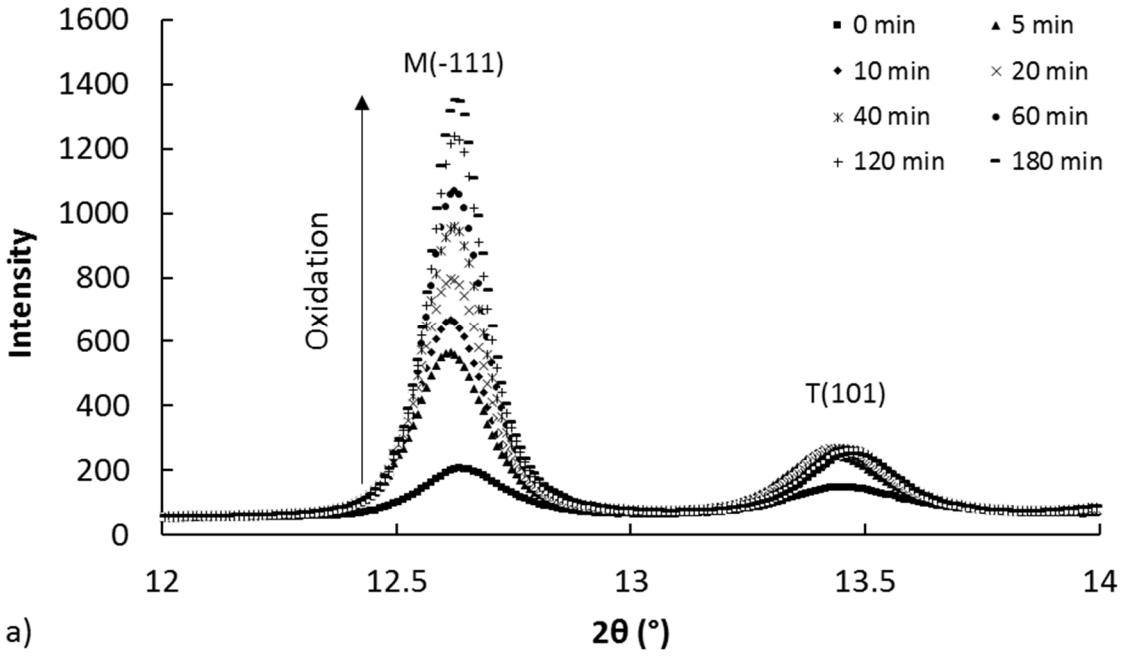
1600
1400
1200
1000
800
600
400
200
0
Intensity
M(-111)
Oxidation
T(101)
0 min
5 min
10 min
20 min
40 min
60 min
120 min
180 min
12
12.5
13
13.5
14
2θ (°)

a)

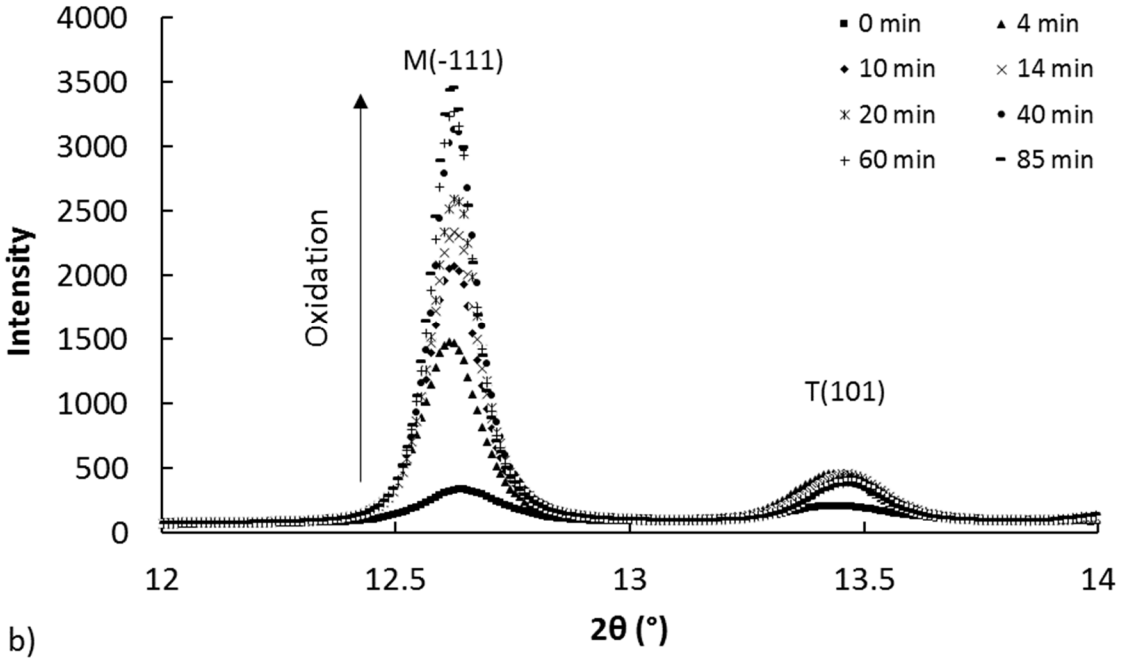
4000
3500
3000
2500
2000
1500
1000
500
0
Intensity
M(-111)
Oxidation
T(101)
0 min
4 min
10 min
14 min
20 min
40 min
60 min
85 min
12
12.5
13
13.5
14
2θ (°)

b)

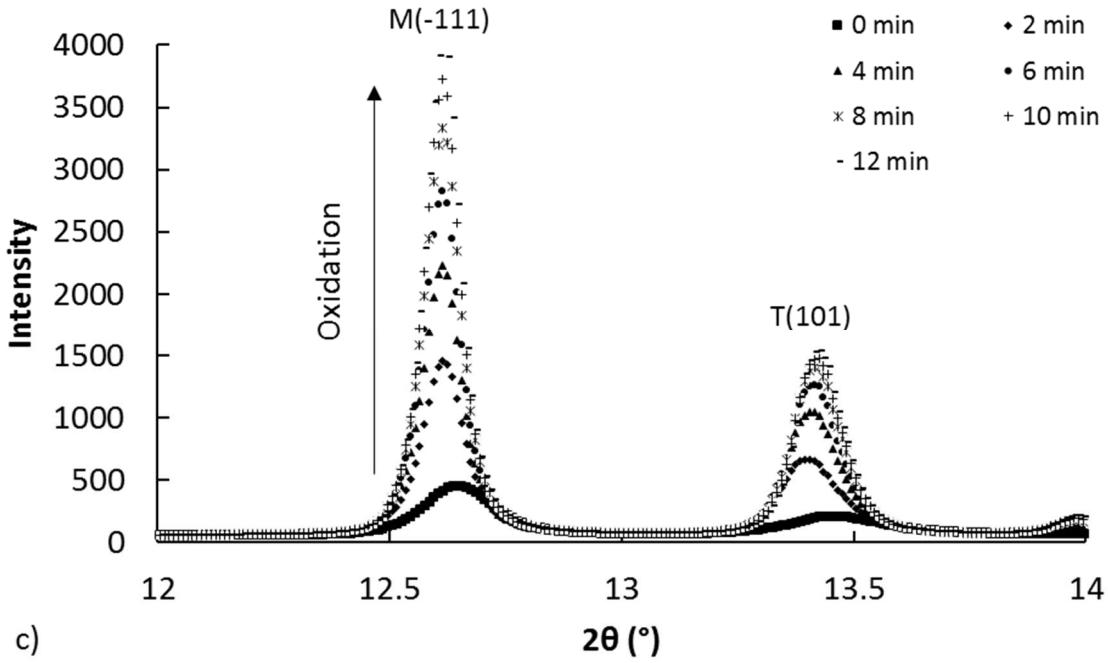

Fig. 6. Diffraction patterns obtained at various times during oxidation under 90 vol% He-10 vol% O_2 at approximately a) 700°C, b) 800°C and c) 900°C.

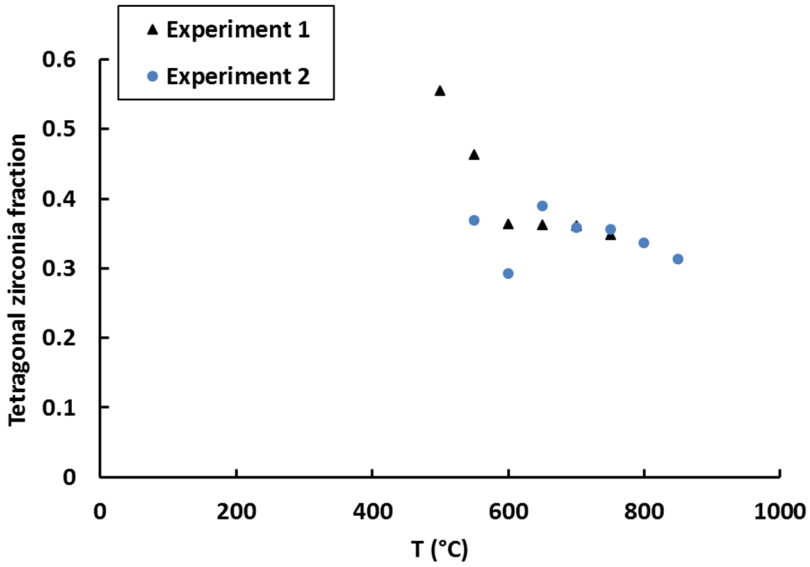

Fig. 7. Tetragonal zirconia phase volume fraction versus temperature during step-heating (two experiments performed with the same heating conditions: 20°C/min heating rate, 2 min-long isothermal steps every 50°C).

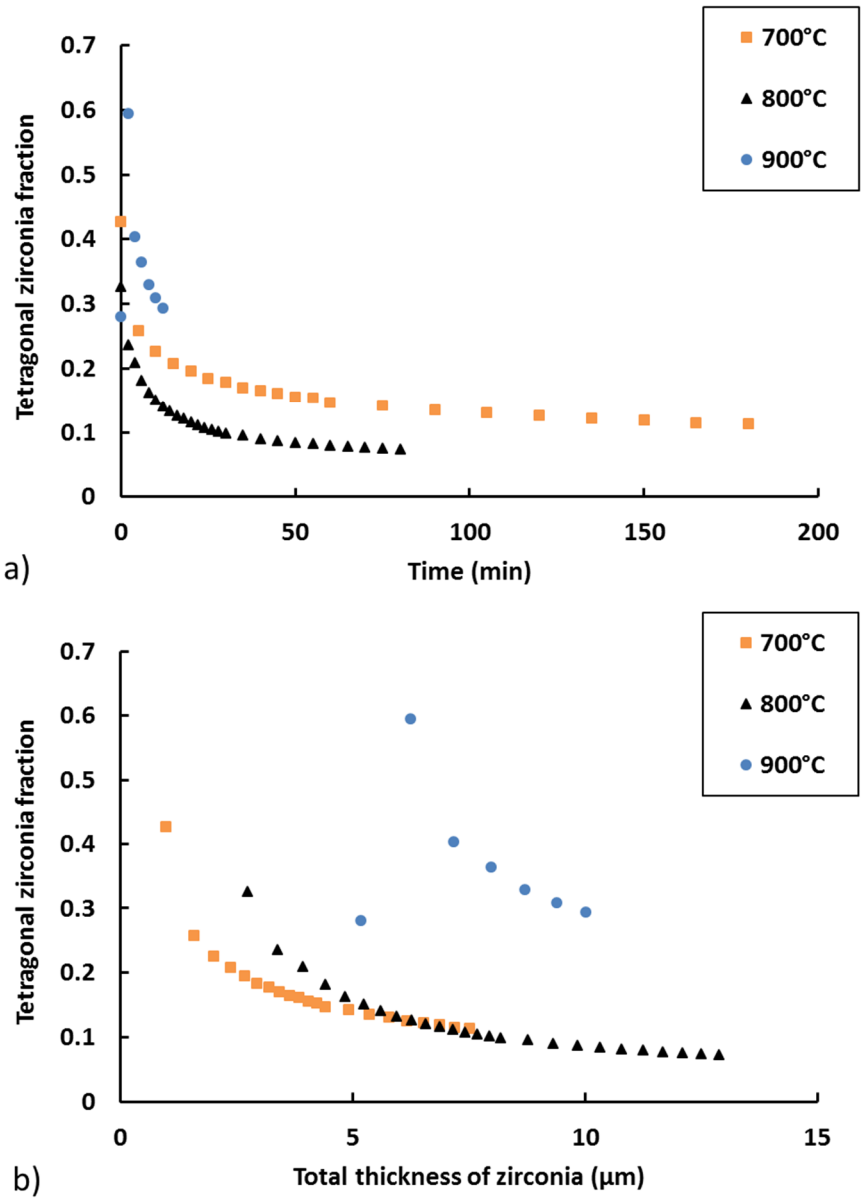

Fig. 8. Tetragonal zirconia phase volume fraction versus a) time and b) total thickness of zirconia obtained during oxidation under 90 vol% He-10 vol% O_2 for samples oxidized 180 min at about 700°C, 75 min at about 800°C and 15 min at about 900°C.

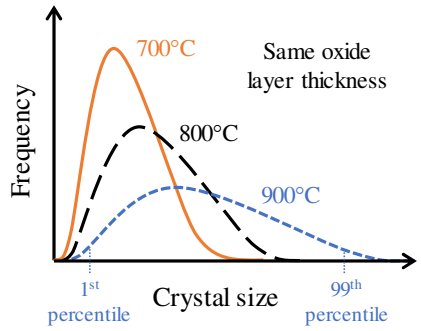

Fig. 9. Schematic representation of the crystal size distribution for oxide layers with similar thicknesses formed at 700, 800 and 900°C.

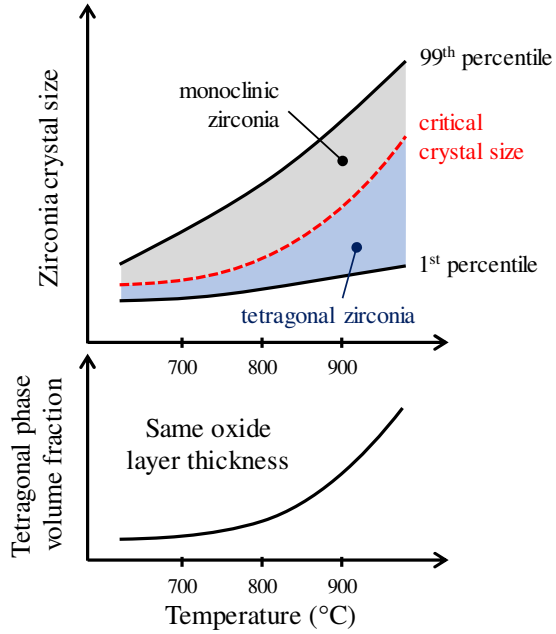

Fig. 10. Schematic representation of the expected evolution of zirconia crystal size (1st and 99th percentiles of the crystal size distribution), critical crystal size below which tetragonal zirconia can be stabilized and volume fraction of the tetragonal phase of zirconia as a function of oxidation temperature, for a given oxide layer thickness.

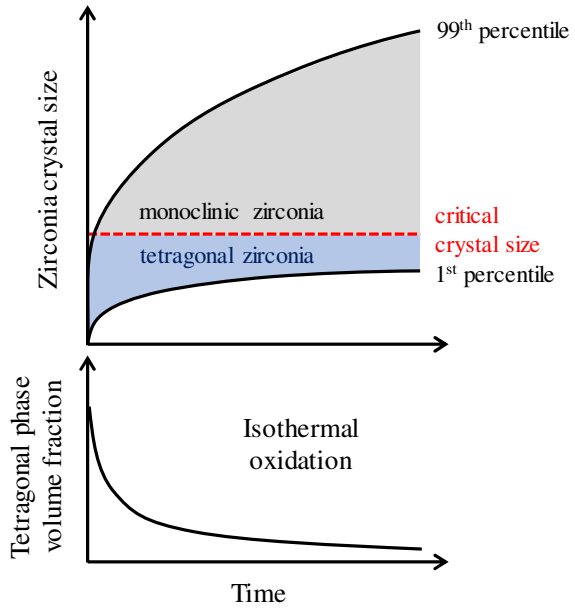

Fig. 11. Schematic representation of the expected evolution of zirconia crystal size (1st and 99th percentiles of the crystal size distribution), critical crystal size below which tetragonal zirconia can be stabilized and volume fraction of the tetragonal phase of zirconia as a function of oxidation time at a given temperature.

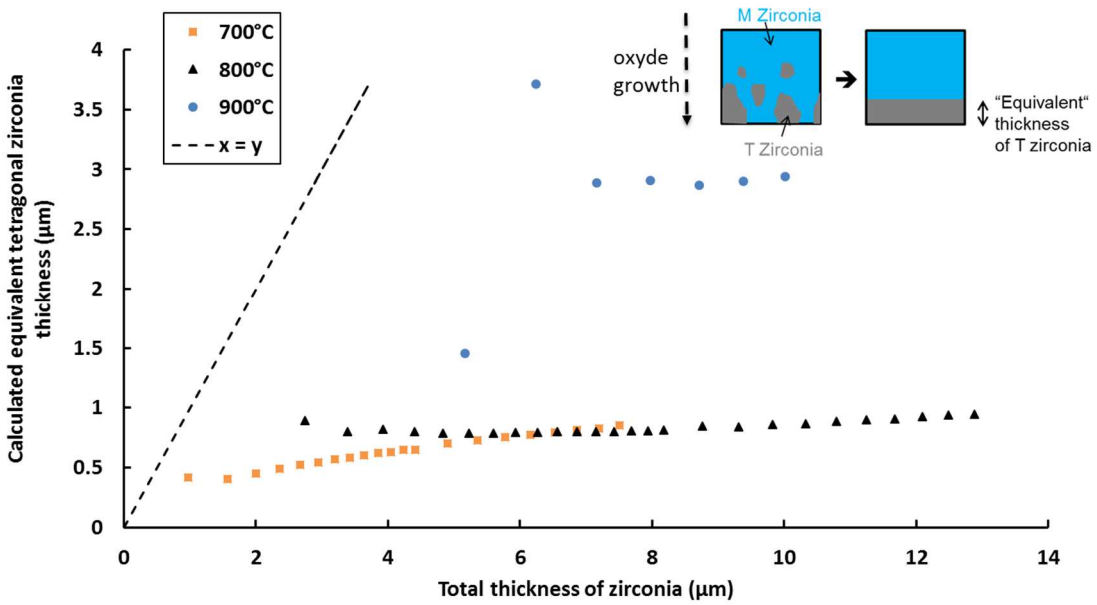

Fig. 12. "Equivalent" tetragonal zirconia thickness versus the expected total thickness of zirconia obtained during oxidation for samples oxidized 180 min at about 700°C, 85 min at about 800°C and 12 min at about 900°C.

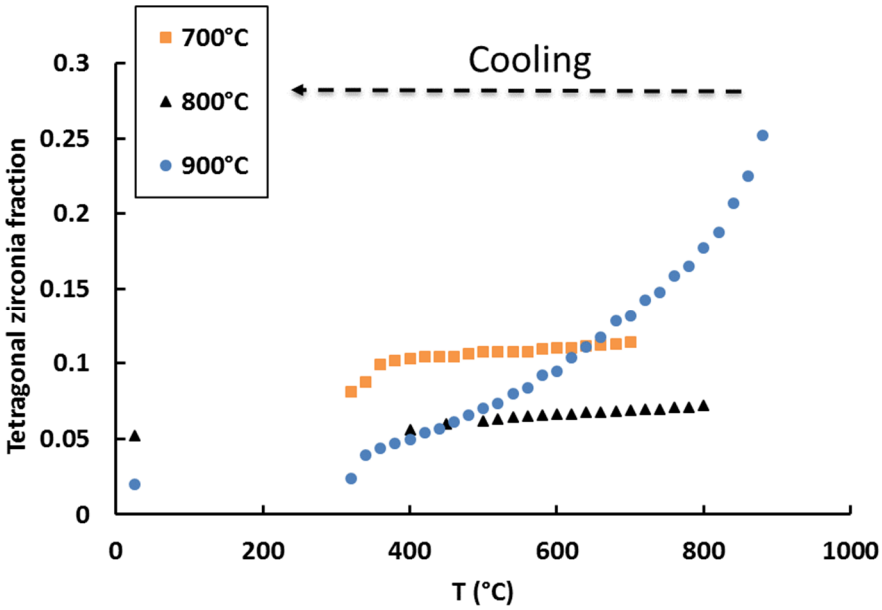

Fig. 13. Tetragonal zirconia phase volume fraction versus temperature during step-cooling for samples oxidized 180 min at about 700°C, 85 min at about 800°C and 12 min at about 900°C.